Supporting Information

Self-Healing Polymer Dielectric Exhibiting Ultrahigh Capacitive Energy Storage Performance at 250 °C

*Wenhan Xu, Fei Yang, Guodong Zhao, Shixian Zhang, Guanchun Rui, Muchen Zhao, Lingling Liu, Long-Qing Chen, and Qing Wang**

Dr. W. Xu, Dr. F. Yang, Dr. S. Zhang, Dr. G. Rui, M. Zhao, Dr. L. Liu, Prof. L.-Q. Chen and Prof. Q. Wang

Department of Materials Science and Engineering, The Pennsylvania State University, University Park, Pennsylvania 16802, USA

E-mail: wang@matse.psu.edu

Experimental procedures

Materials

4-Methylsulfonylaniline, 4-dimethylaminopyridine (DMAP), norbornene-5,6-*endo*-dicarboxylic anhydride and were purchased from VWR. The solvent Dipropylene glycol dimethyl ether (DMM), *N*,*N*-dimethylformamide (DMF) were purchased from Sigma-Aldrich. BCB monomers and *b*-staged BCBs (partially polymerized) with the number average molecular weight of ~25,000 were supplied by Dow Chemical.

Synthesis of monofunctional monomers (N-4-aminophenyl sulfonylmethyl-norbornene imide, SNI)

A solution containing 4-methylsulfonylaniline (3.44 g, 20 mmol) in 30 ml toluene was slowly added to a stirred solution of norbornene-5,6-endo-dicarboxylic anhydride (3.92 g, 24 mmol) in 100 ml toluene. DMAP (0.488 g, 4 mmol) was then added at room temperature, and the mixture was stirred at 110 °C for 12 hours (as shown in Figure S11a). After cooling, the reaction mixture was poured into excess water and filtered to isolate a solid. The solid was further purified by column chromatography on silica gel, using CH_2Cl_2/CH_3OH (10:1) as the eluent, yielding solid SNI (5.7 g, 86% yield).

Copolymer films Preparation Characterization

SNI monomer was dispersed in DMM at a concentration of 0.05 mmol mL^{-1}. Then, 0.5 mmol of BCB monomers was dissolved in 2 ml of DMM and stirred for 8 hours. Afterward, the SNI DMM solution was mixed with the BCB solution in a certain ratio. The mixture was stirred for 1 hour and then sonicated for 30 minutes. Next, the mixture was drop-cast onto a glass slide and baked at 120 °C for 12 hours, followed by curing at 250 °C for 24 hours under vacuum. During this process, the D-A reaction occurred, forming a copolymer as shown in Figure S11b. After

soaking in water for 1 day, the film was peeled off. The film's thickness can be adjusted by varying the concentration of the cast solution. In this study, the copolymers are named according to the molar ratio of the feed. *c*BCB-*co*-SNI specifically refers to copolymers with 5 mol% SNI content. The SNI contents of *c*BCB-*co*-SNI-2.5, *c*BCB-co-SNI-5, *c*BCB-*co*-SNI-7.5, and *c*BCB-*co*-SNI-10 are 2.5 mol%, 5 mol%, 7.5 mol%, and 10 mol%, respectively.

Characterization

TA Instrument Q2000 differential scanning calorimeter was used to conduct Differential Scanning Calorimetry (DSC) at a heating/cooling rate of 10 °C per minute. Gold and Aluminum electrodes, 2.6 mm in diameter and 60 nm thick, were deposited on both sides of the films for electrical measurements. Dielectric spectra were obtained between 25 °C and 270 °C, and from 100 Hz to 1 MHz, using a Keysight 4980A LCR meter equipped with an oven. Conduction current was measured under various electric fields using a Trek 10/10B-HS amplifier and a Delta Design 9010 oven. The electrical breakdown strength was assessed using a Trek 610E amplifier, applying a DC voltage ramp rate of 500 V s^{-1}, and analyzed using the two-parameter Weibull statistic. Electric displacement-electric field (D-E) loops were recorded using a modified Sawyer-Tower circuit with a unipolar triangle voltage at 100 Hz frequency.

Simulation

In this part, we introduce the approach of the numerical calculation to discuss the disorder effect on the electron transmission behavior within the single-particle hopping model. As we mentioned in the main text, topologically, the conduction model of the hopping motion of localized electrons in dielectric structures of Fig. 1ab is equivalent to a two-dimensional hopping model shown in Figure 1c. In this situation, we can calculate the transmission coefficient of electrons in the structure of Figure 1c to elucidate the disorder effect.

The total Hamiltonian H of electrons in Figure 1c can be described by the tight-binding Hamiltonian with the nearest-neighbor approximation[S1]:

$$H = H_c + H_L + H_R + H_{CL} \quad (1)$$

where H_C denote the Hamiltonian of the center structure; $H_{L,R}$ are the Hamiltonian of the left and right leads, respectively; H_{CL} stands for the couplings between the structure and leads. These terms are written as

$$H_c = \sum_i U_i c_i^\dagger c_i - \sum_{<i,j>} t c_i^\dagger c_j \quad (2)$$

$$H_\alpha = \varepsilon_0 \sum_{i\alpha} c_{i\alpha}^\dagger c_{i\alpha} - t \sum_{<i_\alpha, j_\alpha>} c_{i\alpha}^\dagger c_{j\alpha},\ \alpha = L, R \quad (3)$$

$$H_{CL} = -t \sum_{\alpha=L,R} \sum_{<i_\alpha,\, i_s>} \left(c_{i\alpha}^\dagger c_{js} + H.c. \right) \quad (4)$$

Here, the index *i* is the site coordinate in the structure and leads; <*i*, *j*> denotes that the summation is restricted to the nearest neighbors with the connection; $\varepsilon_0 = 4t$ represents the on-site energy in leads (metal electrode in this simulation model).

Within the framework of the Landauer-Buttiker approach[S1,S2], the electron transmission coefficient around local disorder is given by

$$T(E) = T_r[\Gamma_L(E) G_C^R(E) \Gamma_R(E) G_C^A(E)] \quad (5)$$

where $G_C^R = [E - H_c + i0^+]^{-1}$ and $G_S^A = [E - H_c + i0^+]^{-1}$ denote the retarded and advanced Green's function of the center structure[1]; E is the kinetic energy of electron from the electrode, and we set $E = 0.4t$ in the present work; $\Gamma_{L/R} = i[\sum_{L/R}^R - \sum_{L/R}^A]$ with $\sum_{L/R}^R = \tau_{L/R}^\dagger g_{L/R}^R \tau_{L/R}$ and $\sum_{L/R}^A = \tau_{L/R}^\dagger g_{L/R}^A \tau_{L/R}$ being the retarded and advanced surface self-energies due to the coupling with the isolated ideal leads. The implementation of these contact self-energies requires for the lead surface Green functions $g_{L/R}$ and contact tunneling matrix $\tau_{L/R}$, which can be determined through the iterative solution scheme within the recursive Green function methods[S3].

In the numerical simulation, we first artificially set a four-link connection of SNI into the cross-linked network, as shown in Figure S1a, and calculate the transmission coefficient of this structure (blue curve in Figure 1d and solid curve in Figure S1b). As a consequence of the translational-symmetry breaking, both positive and negative on-site energy difference between disorder site and normal site are detrimental to the conducting behavior, leading to the decrease of transmission coefficient, as mentioned in the main text. Then, we consider the single-link connection of SNI. As seen from Figure S1c and S1e, there are two cases for the remaining link of SNI: (i) along and (ii) perpendicular to the transport direction, respectively. We separately calculate the transmission coefficient for each case (shown by solid curve in Figure S 1d and S1f), and at both cases, sharp anti-resonance of the electron conduction emerges in the regime of negative U due to the emerging Fano-type anti-resonance [S4,S5] by strongly localized state, which is a unique character by the single-link connection as mentioned in the main text. Particularly, in comparison to the case with the remaining link of SNI perpendicular to the transport direction, the maximum peak of the electric-transmission gets remarkably suppressed when the remaining link of SNI is along the transport direction. Actually, both cases exist in the realistic material, so we take an average of the conduction on both cases in the main text (shown by red curve in Figure 1d).

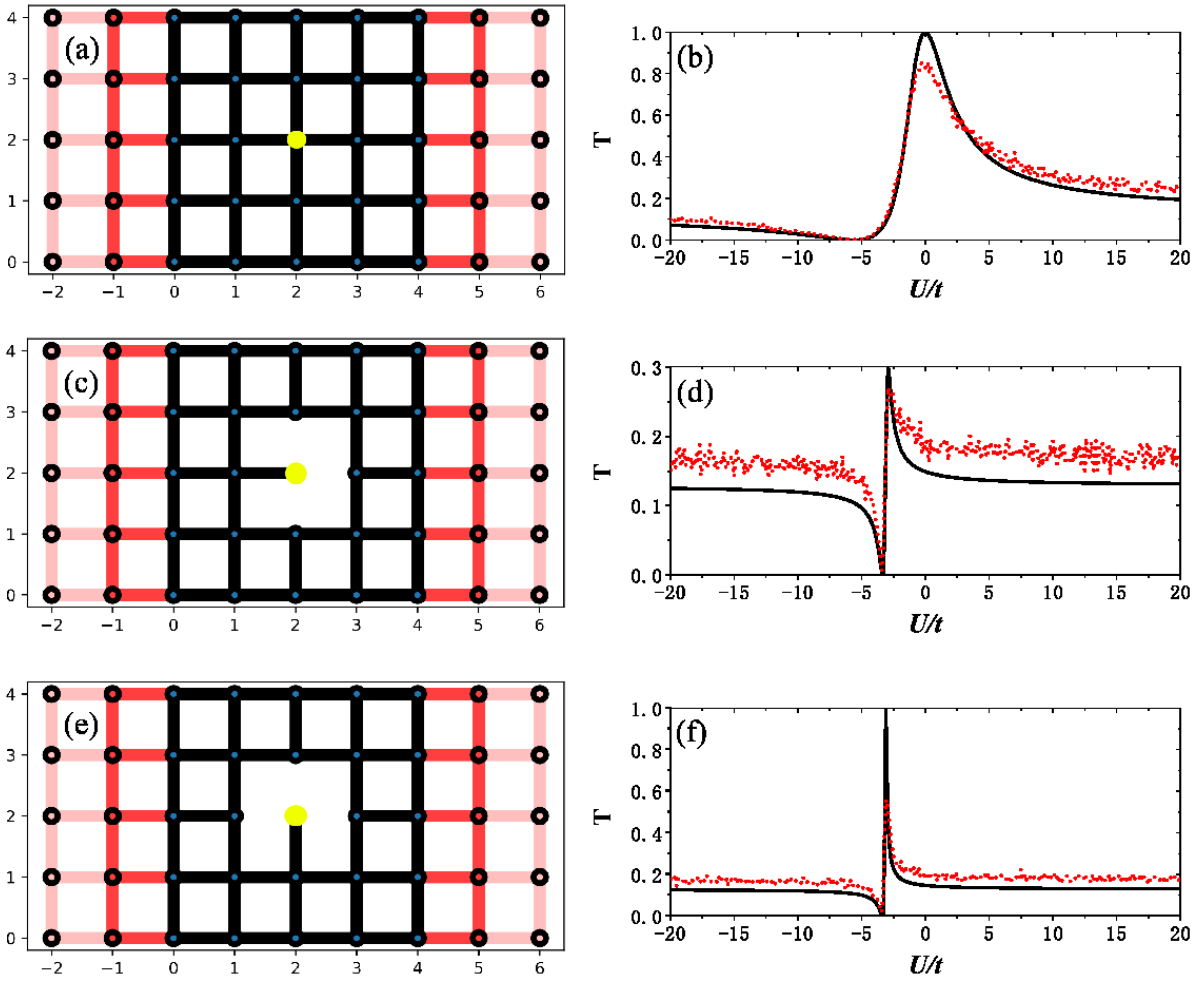

Figure S1. (Color online) Schematic illustration of a two-dimensional single-particle hopping model with tangent connection to the lead (red part) and the correspondingly calculated electron transmission coefficient. (a): four-link connection of SNI into the cross-linked network; (c) and (e): single-link connection of SNI into the cross-linked network. The blue dots and black part denote the cross-linked network formed by pristine *c*BCB and the yellow dot stands for the monofunctional copolymer monomer which serves as an internal disorder site. (b), (d) and (f): numerically calculated transmission coefficient vs on-site energy of the disorder for structures of (a), (c) and (e), respectively. Solid curve: results without hopping fluctuation; Dots: results with random fluctuation on nearest-neighbor hopping strength after the average over 100 random configurations for each structure.

Finally, we justify that as a consequence of the Anderson disorder localization, the electric-transmission coefficient reduction by the unique translational-symmetry breaking from SNI is robust against structure distortion/dislocation (i.e., fluctuation of hopping or on-site energy on

normal sites) and disturbance by external field as well as thermal fluctuation. The robustness of the electric transmission reduction due to the localization/Fano effect against disturbance by external field has been demonstrated in the previous work [S6]. In the present work, we consider a hopping fluctuation by generating random hopping strength $t_{ij} = t + \delta t$ at each nearest neighbor with the connection [here, $\delta t = W\xi$ with ξ being a random number with a uniform probability distribution in the range (−1, 1) and W is the strength of fluctuation], which can describe the soft character of cross-linked network formed by cBCB as well as thermal fluctuation. By setting a large fluctuation W = 0.2t, we calculate the transmission amplitudes averaged over 100 random configurations for each structure in Figure S1a, S1c and S1e, and the corresponding numerical results are shown by red dots in Figure S1b, S1d and S1f. As seen from the figure, for each structure, the transmission coefficient reduction by disorder effect exhibits strong robustness against the large hopping fluctuation.

Last but not least, the model presented above in fact concerns the transmission coefficient of electrons around single local disorder, which gets remarkably reduced as a consequence of the Anderson localization effect. Consequently, this reduction effect in fact suppresses the hopping distance around single local disorder, as mentioned in the main text. One can naturally expect the reduction of the macroscopic electric conductivity for the realistic case with finite concentration, considering the random phase approximation for the random distribution of the disorders[S7].

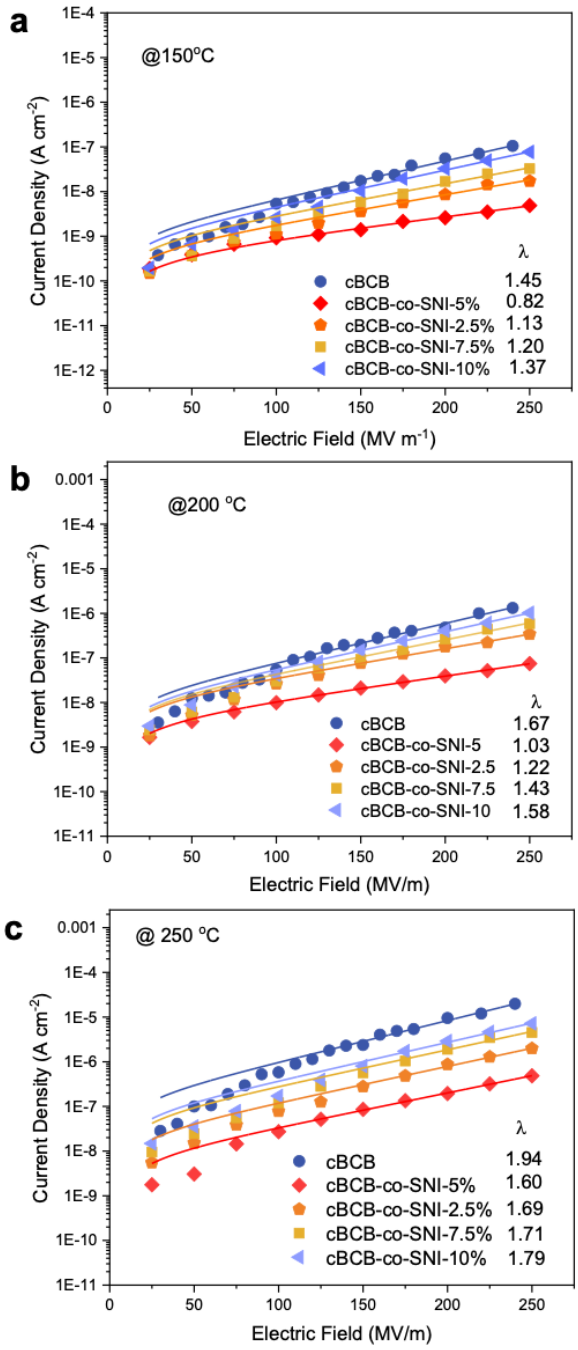

Figure S2. Electric field-dependent conduction current density of *c*BCB and *c*BCB-*co*-SNI copolymer (a) at 150 °C, (b) at 200 °C, (c) at 250 °C.

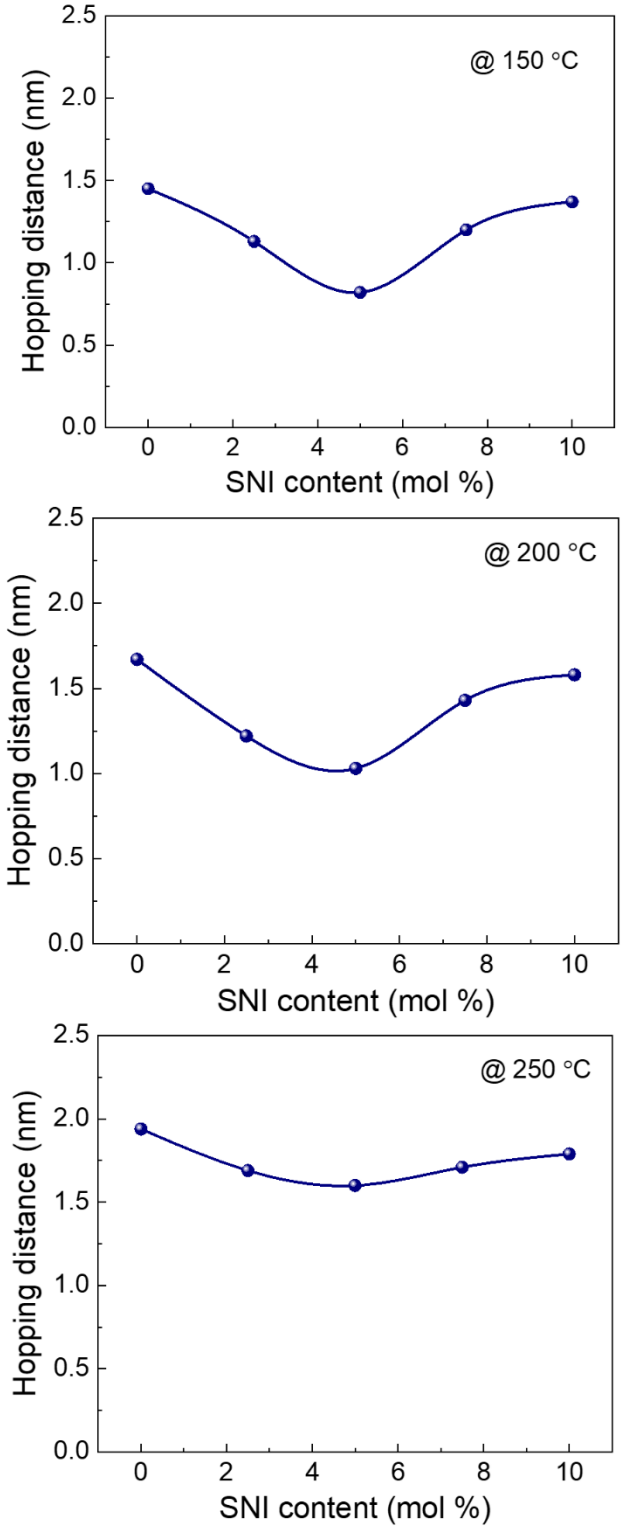

Figure S3. Charge carrier hopping distance of *c*BCB and *c*BCB-*co*-SNI copolymer at 150 °C, at 200 °C and at 250 °C.

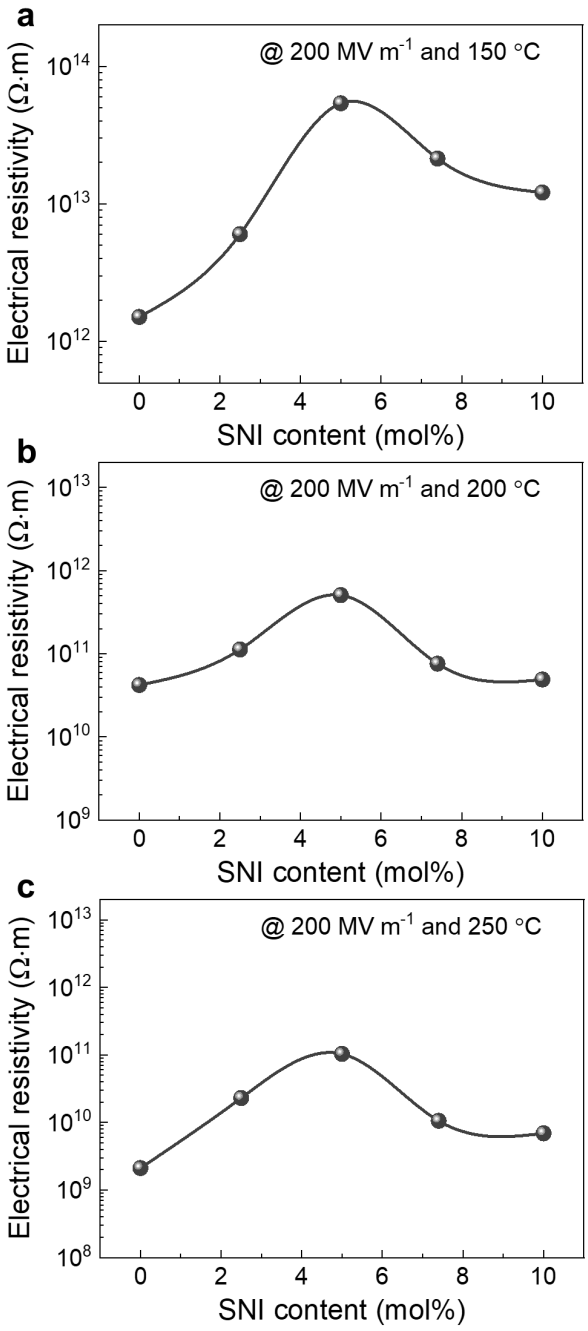

Figure S4. Electrical resistivity of *c*BCB and *c*BCB-*co*-SNI copolymer at 150 °C, 200 °C and 250 °C.

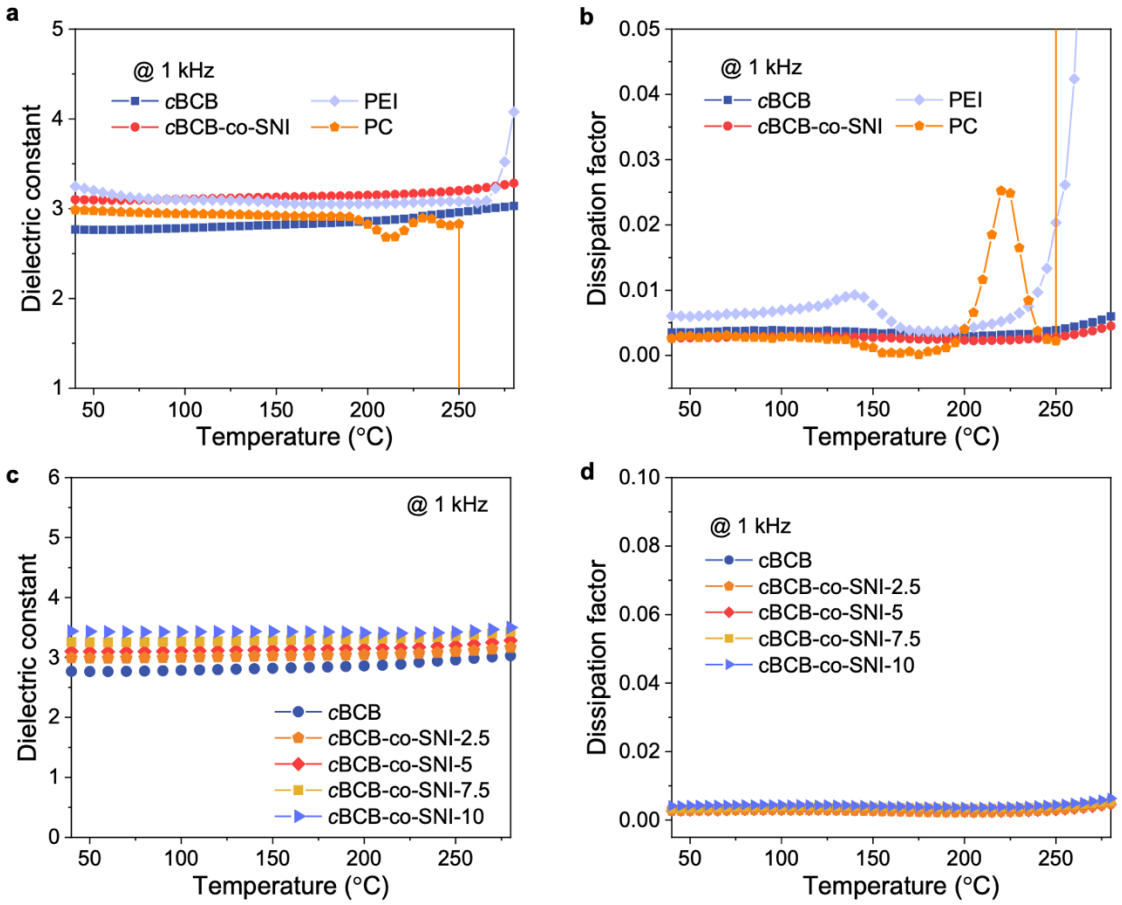

Figure S5. Temperature-dependent a,c, dielectric constant and b,d, dissipation factor of *c*BCB and cBCB-*co*-SNI copolymers at 1kHz.

The dielectric constant of the copolymer has increased compared to the original cBCB because the SNI group contains strongly polar groups such as carbonyl and sulfone. Additionally, breaking the symmetry of the original polymer crosslinking network improves the mobility of dipoles within the molecular chains. The dissipation factor, however, shows an initial decrease followed by an increase with the addition of SNI, reaching an optimal value in cBCB-co-SNI-5. This is because a small amount of SNI can reduce the conductivity of copolymer, increase the flexibility of the overall network, and reduce dipole movement losses. However, SNI inherently has a higher dissipation factor than BCB, so an excessive amount of SNI increases the dissipation factor of the copolymer.

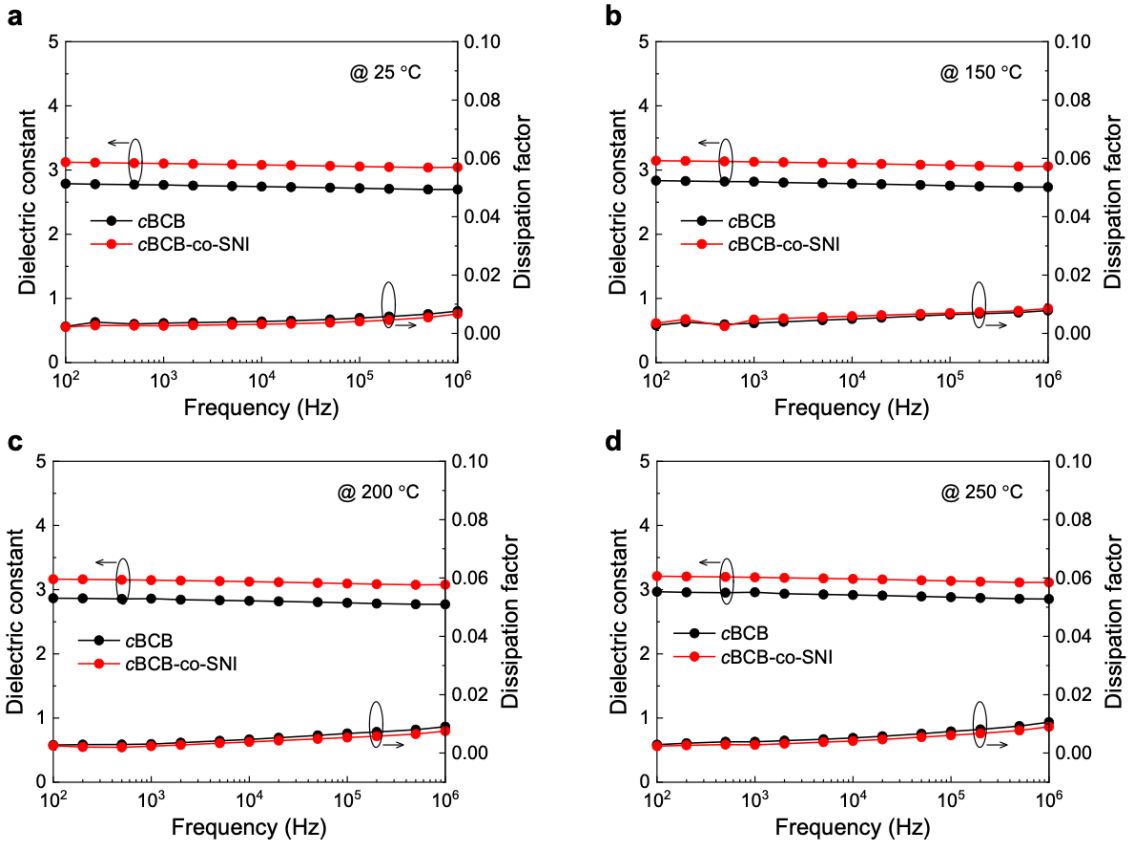

Figure S6. Frequency-dependent dielectric constant and dissipation factor of *c*BCB and *c*BCB-*co*-SNI at different temperatures.

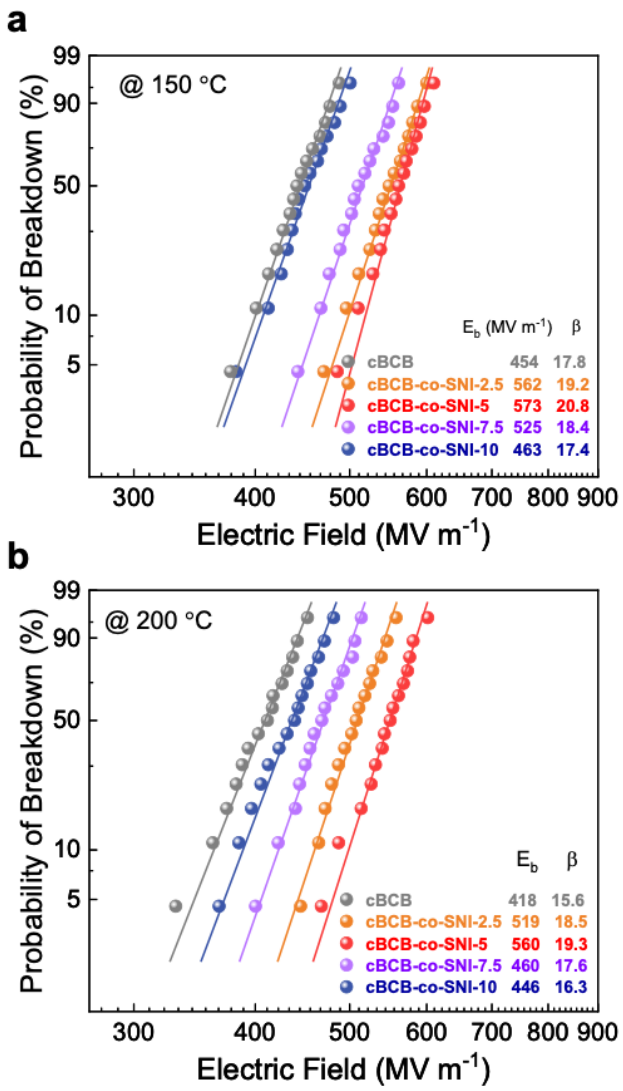

Figure S7. Breakdown strength of *c*BCB-*co*-SNI and *c*BCB at 150 °C and 200 °C.

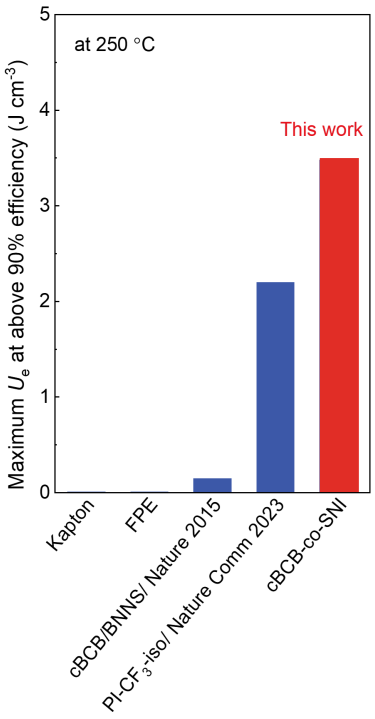

Figure S8. Comparison of the discharged energy density at ≥90% charge–discharge efficiency of cBCB-co-SNI and other high-temperature dielectric polymers and composites at 250 °C.

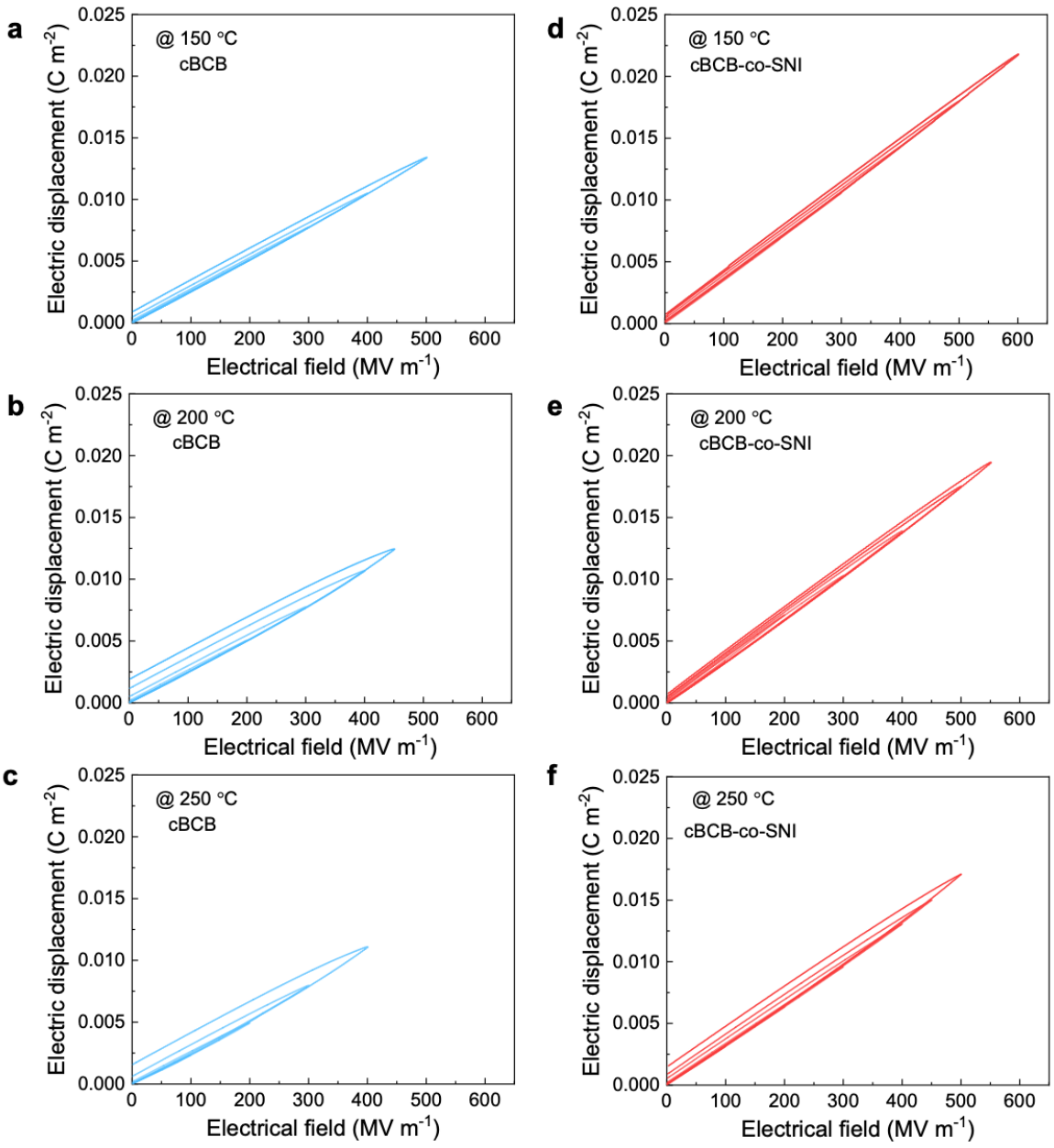

Figure S9. *D-E* loops of *c*BCB and *c*BCB-*co*-SNI at a,b, 150 °C, c,d, 200 °C and e, f, 250 °C.

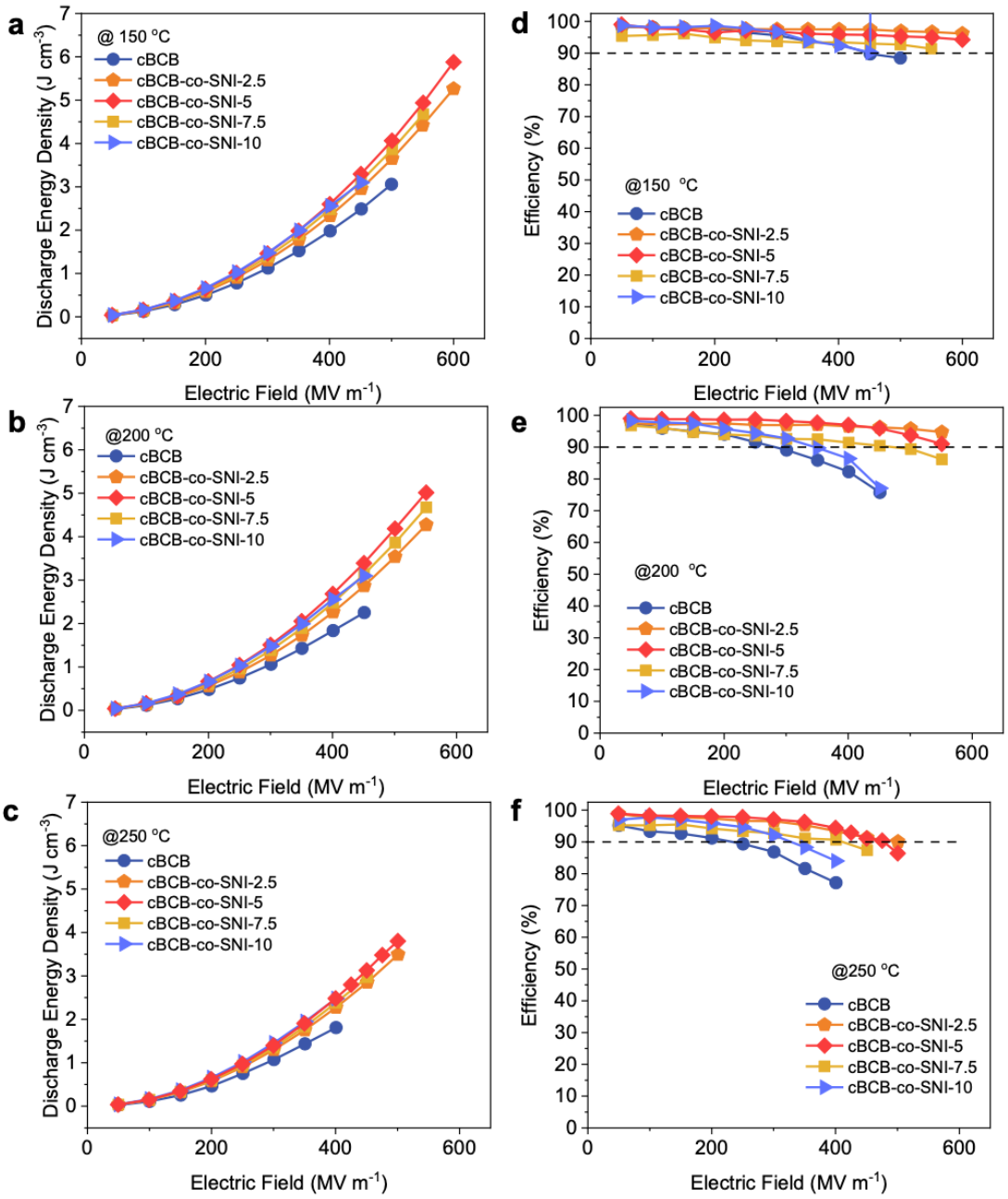

Figure S10. Discharged energy density (a,b,c) and charge-discharge efficiency (d,e,f) of *c*BCB and *c*BCB copolymers measured at a, d 150 °C, b,e, 200 °C, and c,f 250 °C.

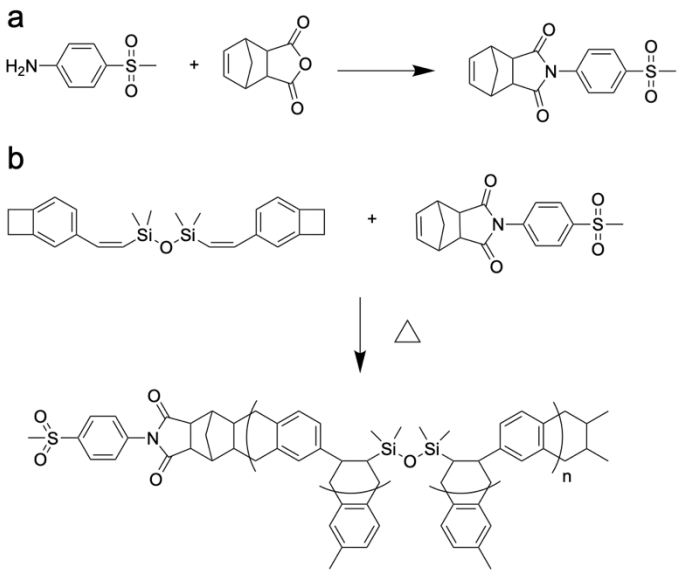

Figure S11. Synthesis of monomers and copolymers. (a) SNI. (b) *c*BCB-*co*-SNI.

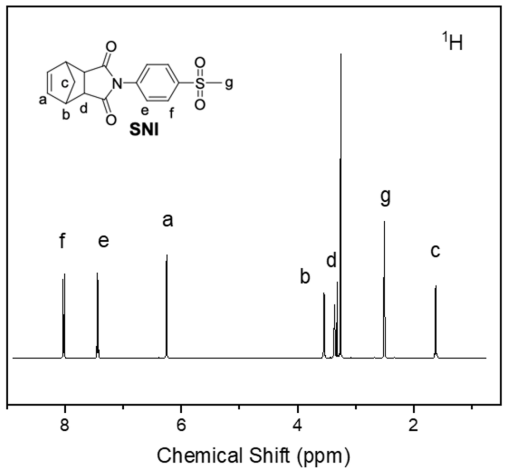

Figure S12. ^{1}H NMR spectra of SNI in DMSO-d6.

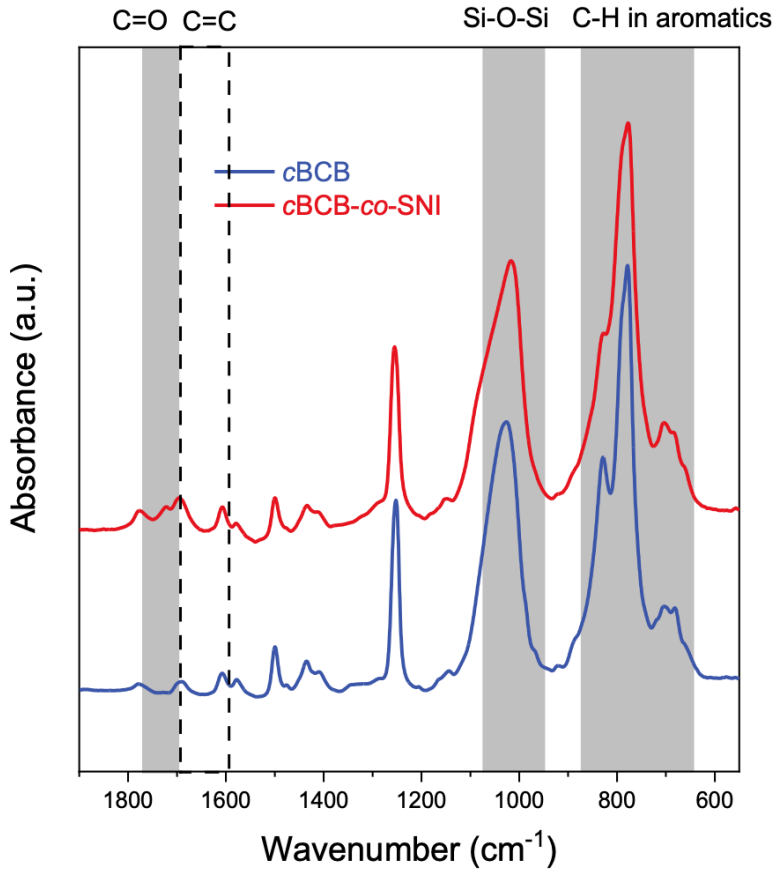

Figure S13. ATR-FTIR spectra of polymer films of *c*BCB and *c*BCB-*co*-SNI. In the cBCB-co-SNI film, the appearance of a carbonyl peak at 1720 cm^{-1} confirms the presence of SNI. Meanwhile, the absence of new carbon-carbon double bond peaks in the region of 1600-1700 cm^{-1} indicates that the SNI monomer has reacted, and its double bonds are not retained in the newly prepared film.

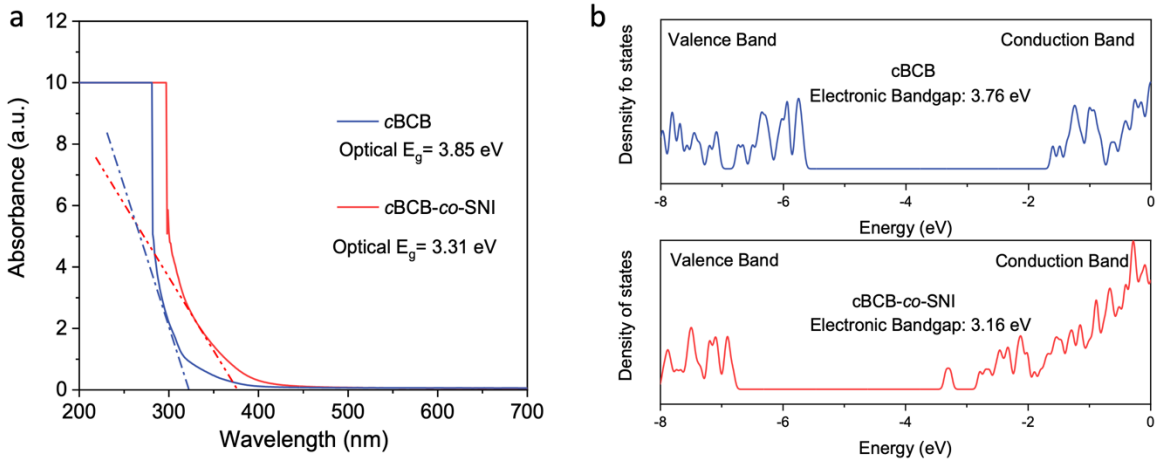

Figure S14. (a) UV–vis spectra of cBCB and cBCB-co-SNI, Optical E_g represents the experimental optical bandgap. (b) Calculated density of states (DOS) and the corresponding computed electronic bandgap of cBCB and cBCB-co-SNI, where zero energies are referenced to the average vaccum levels.

The optical bandgap is determined using the equation, E_g (eV) = 1240 / λ_g, where λ_g represents the cut-off wavelength at the onset of absorption in the linear region. The experimentally measured optical E_g values exhibit a consistent trend with the electronic E_g values calculated via Density Functional Theory (DFT).

The density-functional-theory calculation was performed using the Vienna Ab initio Simulation Package (VASP) [S8,S9] with projected-augmented-wave method. The exchange-correlation functional is Perdew, Burke, and Ernzerhof's approach of generalized gradient approximation [S10]. We apply the van der Waals dispersion correction via DFT-D3 method with Becke-Johnson damping function [S11,S12], and only consider its 1D periodic imaging. The energy cutoff for the plane-wave basis set is set to 600 eV. The atom coordinates and the lattice constant *c* along the molecular chain are relaxed until all the forces are smaller than 0.05 eV/Å. Dipole correction is considered along the *b*-axis [S13]. Due to the large size of unit cells, one gamma point is taken for k-point sampling. We approximate the concerned polymers by building simplified molecular chains with the characteristic clusters of cBCB and cBCB-co-SNI. To avoid inter-chain interactions, we build vacuum layer thicker of 15~20 Å on *a*- and *b*-directions.

The peak around -3.1 eV of cBCB-co-SNI in the figure S14 is attributed to the carbonyl group on SNI. The copolymer calculated here has one SNI in each structural unit, so the peak is much larger than the actual copolymer in this work. If this orbital is ignored, the bandgap size of copolymer is 3.71 eV.

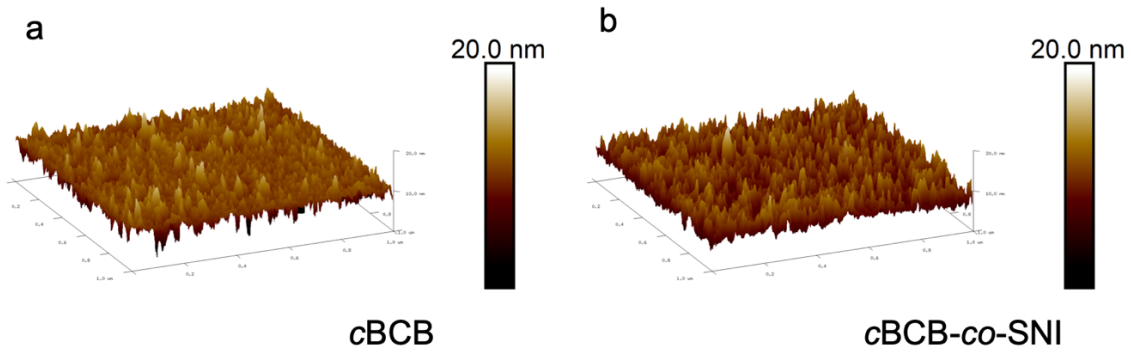

Figure S15. AFM surface topography of (a) *c*BCB and (b) *c*BCB-*co*-SNI

We performed surface AFM tests on the original cBCB and the copolymer films. The results show that the surface roughness of both films is quite similar, with height variations of less than 20 nm. The scales in the figure are one micron.

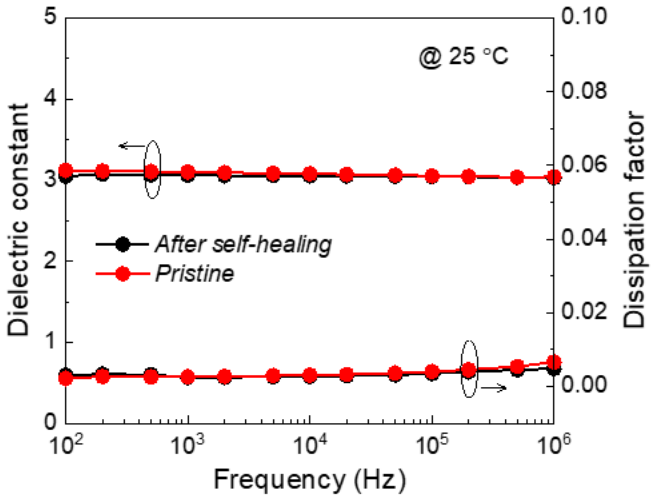

Figure S16. Frequency-dependent dielectric constant and dissipation factor of cBCB-co-SNI before and after self-healing.

Table S1 the applications of high-temperature dielectric polymer film capacitors

Application	Temperature	Reference
Pulsed power system	120-180 ºC	[S14]
Automobile	140-150 ºC	[S15]
Oil & gas exploration	170-250 ºC	[S16]
Electrified aircraft	180-300 ºC	[S17]
Geothermal	200-300 ºC	[S18]

Supporting References

[S1] S. Datta, *Electronic Transport in Mesoscopic Systems*, Cambridge University Press, Cambridge, **1995**.
[S2] M. Büttiker, *Phys. Rev. Lett.* **1986**, *57*, 1761.
[S3] C. H. Lewenkopf, E. R. Mucciolo, *J Comput Electron* **2013**, *12*, 203.
[S4] U. Fano, *Phys. Rev.* **1961**, *124*, 1866.
[S5] A. E. Miroshnichenko, S. Flach, Y. S. Kivshar, *Rev. Mod. Phys.* **2010**, *82*, 2257.
[S6] F. Yang, M. W. Wu, *Journal of Applied Physics* **2014**, *116*, 083701.
[S7] V. Ambegaokar, B. I. Halperin, J. S. Langer, *Phys. Rev. B* **1971**, *4*, 2612.
[S8] G. Kresse and J. Furthmüller, Phys. Rev. B **54**, 11169 (1996).
[S9] G. Kresse and J. Furthmüller, Comp. Mater. Sci. **6**, 15 (1996).
[S10] J. P. Perdew, K. Burke, and M. Ernzerhof, Phys. Rev. Lett. **77**, 3865 (1996).
[S11] S. Grimme, J. Antony, S. Ehrlich, and H. Krieg, J. Chem. Phys. **132**, 154104 (2010).
[S12] S. Grimme, S. Ehrlich, and L. Goerigk, J. Comput. Chem. **32**, 1456 (2011).
[S13] J. Neugebauer and M. Scheffler, Phys. Rev. B **46**, 16067 (1992).
[S14] E. J. Barshaw, J. White, M. J. Chait, J. B. Cornette, J. Bustamante, F. Folli, D. Biltchick, G. Borelli, G. Picci, and M. Rabuffi, *IEEE Transactions on Magnetics*, 2007, **43**, 223–225.
[S15] R. W. Johnson, J. L. Evans, P. Jacobsen, J. R. Thompson and M. Christopher, *IEEE transactions on electronics packaging manufacturing*, 2004, **27**, 164–176.
[S16] J. Watson and G. Castro, *Analog Dialogue*, 2012, **46**, 3–9.
[S17] J. A. Weimer, in *[1993 Proceedings] AIAA/IEEE Digital Avionics Systems Conference*, 1993, pp. 445–450.
[S18] H. Li, Y. Zhou, Y. Liu, L. Li, Y. Liu and Q. Wang, *Chem. Soc. Rev.*, 2021, **50**, 6369.